Stopping of swift antiprotons by hydrogen atoms and the Barkas correction

Remigio Cabrera-Trujillo and John R. Sabin
Department of Physics, University of Florida, Gainesville, Florida 32611, USA

Yngve Öhrn and Erik Deumens
Department of Chemistry, University of Florida, Gainesville, Florida 32611, USA
(Received 4 August 2004; published 18 January 2005)

We report calculations of the stopping cross sections of hydrogen atoms for protons and antiprotons at low to intermediate energies and take the difference explicitly to determine the Barkas correction for this system. The calculational method used is the electron-nuclear dynamics formalism which involves the coupled direct dynamics of all nuclei and electrons and thus includes all terms in the Born expansion. The formalism is a nonperturbational, *ab initio* approach to solve the time-dependent Schrödinger equation, applicable to all the projectile energies under consideration. This is in contrast to the use of different velocity-dependent models for different energy ranges used in other approaches. We find that at high projectile energies, target excitation and ionization are responsible for the projectile energy loss. However, at low projectile energies, the repulsion of the negatively charged projectile and the target electronic structure and its coupling to the target nuclei produce a billiard ball effect which combined with the large ionization and excitation induced by the antiproton is responsible for the large nuclear stopping power, contrary to near-adiabatic dynamics predicted by other models.

DOI: 10.1103/PhysRevA.71.012901 PACS number(s): 34.50.Bw

I. INTRODUCTION

There has been interest in the physics of the interaction of swift ions with matter since the earliest part of the 20th century when the physics of ion-matter interactions first began to be explored [1,2]. The earliest atomic-level explanation of energy deposition, or stopping, was the harmonically bound electron model of Bohr [3,4]. This was followed by the quantum mechanical formulation of stopping of Bethe [5–7], which is still the basis of much of the present day understanding of stopping power.

In Bethe's model, the stopping $-dE/dx$ or energy loss of an incident particle with velocity v per unit path length, can be written

$$-\frac{dE}{dx} = nS(v) = n\frac{4\pi e^4 Z_1^2 Z_2}{mv^2}L(v), \tag{1}$$

where $S(v)$ is the stopping cross section, related to the stopping power by the density of target scattering centers n, and where $L(v)$ is the stopping number. Here Z_2 is the target atomic number. Generally, the projectile is assumed to be stripped with a fixed charge Z_1—that is, no charge exchange is considered [8].

The Bethe theory is developed in the first Born approximation, and thus is limited to terms in the stopping that are proportional to Z_1^2. However, the full Born expansion will, in principle, contain terms in all powers of Z_1. Following Lindhard [9], the stopping number may be expanded in a Born series in the projectile charge as

$$L(v) = \sum_{i=0} Z_1^i L_i(v) \tag{2}$$

where L_0 is the Bethe term ($S \propto Z_1^2$) which includes the shell corrections that arise from violation of Bethe's assumption that the projectile speed is much greater than that of the target electrons.

The second term ($S \propto Z_1^3$) is the first odd term in the Born series, and reflects the asymmetry in energy deposition between charge conjugated particles. The term is referred to as the *Barkas correction* as it was first experimentally demonstrated for muons by Barkas *et al.* in 1963 [10]. It is the determination of this quantity for the hydrogen atom that is the subject of this paper.

II. INTRODUCTION TO THE BARKAS CORRECTION

There have been several attempts to derive an expression for the Barkas correction (for discussions of earlier work, see, e.g., [11,12]). The earlier Barkas correction formulations were made by Jackson and McCarthy [13], and by Ashley, Ritchie, and Brandt (ARB) [14–17], based on the Bohr harmonic model of stopping [3]. More recent studies have been reported by Schiwietz *et al.* [18,19] for He and H_2 targets, by Arista and Lifschitz [20], by Bichsel [21], and by Sigmund and Schinner [22].

Although there have been muon-based experiments on the Barkas effect [10,23], it is the availability of the source at CERN that made antiproton experiments possible [24–26], and made the experimental investigation of the Barkas correction feasible.

From Eqs. (1) and (2), it is apparent that higher terms in Z_1 will be present in an exact calculation of the stopping cross section. In order to accentuate the Barkas effect and higher orders in the stopping cross section, S, it is customary to calculate the relative value of the stopping cross section for the antiparticle with respect to the positive particle, i.e., $\Delta S/S$. Thus, one obtains

$$\frac{\Delta S}{S} = \frac{\sum_{i=0} 2Z_1^{2i+1} L_{2i+1}}{\sum_i Z_1^i L_i} = \frac{2Z_1 L_1 + \cdots}{L_0 + Z_1 L_1 + \cdots}. \tag{3}$$

From Eq. (3), when high-order terms are insignificant (i.e., $L_{2i+1} \ll 1$, $i > 0$), the Barkas term predominates. Furthermore, analysis of Eq. (3) emphasizes the Barkas correction term L_1 at low projectile energies, while the ratio of the stopping cross section between a negative and positive projectile shows only the magnitude of the total contribution. Thus, we require a nonperturbative approach to determine the relative difference in the stopping cross section for a particle and antiparticle colliding with the same target. The approach we use is the electron-nuclear dynamics (END) theory, which is described in the next section.

Of the previous studies, the most complete analysis of the antiproton-hydrogen system to study the Barkas effect has been carried out by Schiwietz *et al.* [19] where they apply three different models depending on the projectile velocity. At low projectile velocities they use the adiabatic-ionization (AI) model based on adiabatic potential curves for the electronic states in the presence of the quasidipole formed by the antiproton and hydrogen nucleus. At higher energies, the distorted-wave (DW) approximation and the atomic-orbital (AO) method are employed around the maximum of the stopping cross section. Thus, although the results shed light on the process of energy loss, the treatment is not consistent for all the projectile energies.

In the next section, we describe the END model which is valid for all the projectile energies below and around the maximum of the stopping cross section.

III. ELECTRON-NUCLEAR DYNAMICS

Our approach to analyzing the energy loss and Barkas effect is based on the application of the time-dependent variational principle (TDVP) to the Schrödinger equation [27], where the wave function is described in a coherent state representation. As the details of the END method have been reported elsewhere [28–30], we present here only a brief description of the fundamental features of the theory.

The TDVP requires that the quantum action

$$A = \int \frac{\langle \xi | i\partial/\partial t - H | \xi \rangle}{\langle \xi | \xi \rangle} dt \tag{4}$$

should be stationary. The use of the variational theory yields the time-dependent Schrödinger equation when variations of the wave function $|\xi\rangle$ over the entire state space are performed. Variation over a subspace yields the TDVP approximation for the time evolution over that subspace of the Schrödinger equation. We use a parametrization of the wave function in a coherent state manifold, which leads to a system of Hamilton's equations of motion [28]. The variational wave function $|\xi\rangle$, is a molecular coherent state

$$|\xi\rangle = |\mathbf{z}, \mathbf{R}, \mathbf{P}\rangle |\mathbf{R}, \mathbf{P}\rangle = |z\rangle |\phi\rangle, \tag{5}$$

where $|z\rangle$ and $|\phi\rangle$ are the coupled electronic and nuclear wave functions, respectively.

The simplest level of the END approach employs a single spin-unrestricted electronic determinant

$$|z\rangle = \det\{\varphi_i(x_j)\} \tag{6}$$

written in terms of the nonorthogonal spin orbitals, φ_i

$$\varphi_i = u_i + \sum_{j=N+1}^{K} u_j z_{ji}, \quad i = 1,2, \ldots, N \tag{7}$$

expressed in terms of a basis $\{u_j\}$ of atomic Gaussian-type orbitals of rank K with complex coefficients $\{z_{ji}\}$. For the Gaussian-type orbital we use

$$u_i = \sum_k c_k (x - R_x)^l (y - R_y)^m (z - R_z)^n \exp[-\alpha_k (\mathbf{x} - \mathbf{R})^2 - i\mathbf{P} \cdot (\mathbf{x} - \mathbf{R})], \tag{8}$$

centered on the average positions $\mathbf{R}$ of the participating atomic nuclei and moving with a momentum $\mathbf{P}$. Here, c_k are the contraction coefficients and α_k are the exponents of the Gaussian basis set. This representation takes into account the momentum of the electron explicitly through the use electron translation factors (ETF's) [31]. The particular form of parametrization of $|z\rangle$ with complex, time-dependent coefficients z_{ji} is due to Thouless [32] and is an example of a so called generalized coherent state [33].

The nuclear part of the wave function is represented by localized Gaussians

$$|\phi\rangle = \prod_k \exp\left[-\left(\frac{\mathbf{X}_k - \mathbf{R}_k}{w} \right)^2 + i\mathbf{P}_k \cdot (\mathbf{X}_k - \mathbf{R}_k) \right] \tag{9}$$

or, in the narrow wave-packet limit ($w \to 0$), by classical trajectories $(\mathbf{R}_k, \mathbf{P}_k)$.

Application of the TDVP then yields the dynamical equations [28]

$$\begin{pmatrix} i\mathbf{C} & \mathbf{0} & i\mathbf{C}_\mathbf{R} & i\mathbf{C}_\mathbf{P} \\ \mathbf{0} & -i\mathbf{C}^* & -i\mathbf{C}_\mathbf{R}^* & -i\mathbf{C}_\mathbf{P}^* \\ i\mathbf{C}_\mathbf{R}^\dagger & -i\mathbf{C}_\mathbf{R}^\mathbf{T} & \mathbf{C}_{\mathbf{RR}} & -\mathbf{I} + \mathbf{C}_{\mathbf{RP}} \\ i\mathbf{C}_\mathbf{P}^\dagger & -i\mathbf{C}_\mathbf{P}^\mathbf{T} & \mathbf{I} + \mathbf{C}_{\mathbf{RP}} & \mathbf{C}_{\mathbf{PP}} \end{pmatrix} \begin{pmatrix} \dot{\mathbf{z}} \\ \dot{\mathbf{z}}^* \\ \dot{\mathbf{R}} \\ \dot{\mathbf{P}} \end{pmatrix} = \begin{pmatrix} \partial E/\partial \mathbf{z}^* \\ \partial E/\partial \mathbf{z} \\ \partial E/\partial \mathbf{R} \\ \partial E/\partial \mathbf{P} \end{pmatrix} \tag{10}$$

where the overdot represents differentiation with respect to the time parameter and $E = \Sigma_k P_k^2/2M_k + \langle z|H_{el}|z\rangle/\langle z|z\rangle$ is the total energy of the system. Here, H_{el} is the electronic Hamiltonian which contains the nuclear-nuclear repulsion potential energy. The nonadiabatic coupling terms between the electron and nuclear dynamics are given by

$$\mathbf{C} = \left. \frac{\partial^2 \ln S(\mathbf{z}^*, \mathbf{R}, \mathbf{P}, z, \mathbf{R}', \mathbf{P}')}{\partial \mathbf{z}^* \partial \mathbf{z}} \right|_{\mathbf{R}'=\mathbf{R}, \mathbf{P}=\mathbf{P}'}, \tag{11}$$

$$\mathbf{C}_R = \left. \frac{\partial^2 \ln S(\mathbf{z}^*, \mathbf{R}, \mathbf{P}, z, \mathbf{R}', \mathbf{P}')}{\partial \mathbf{z}^* \partial \mathbf{R}'} \right|_{\mathbf{R}'=\mathbf{R}, \mathbf{P}=\mathbf{P}'}, \tag{12}$$

$$\mathbf{C_{RR}} = -2\,\mathrm{Im}\left.\frac{\partial^2 \ln S(\mathbf{z}^*,\mathbf{R},\mathbf{P},z,\mathbf{R}',\mathbf{P}')}{\partial\mathbf{R}\partial\mathbf{R}'}\right|_{\mathbf{R}'=\mathbf{R},\mathbf{P}=\mathbf{P}'}, \tag{13}$$

and similar definitions for $\mathbf{C_{RP}}$, $\mathbf{C_P}$, and $\mathbf{C_{PP}}$. Here, $S(\mathbf{z}^*,\mathbf{R},\mathbf{P},\mathbf{z},\mathbf{R}',\mathbf{P}')=\langle\mathbf{z},\mathbf{R}',\mathbf{P}'|\mathbf{z},\mathbf{R},\mathbf{P}\rangle$ is the overlap of determinantal states.

From Eq. (10) it is evident that if there is no electron-nuclear coupling, that is, if the **C**'s are zero, then the equation of the third row becomes just the classical trajectory for a particle in the presence of a static screened potential. Thus, the effects of considering the electron-nuclear coupling are described by the full solution of Eq. (10). Furthermore, the use of coherent states avoids the description of the dynamics in terms of partial waves.

Solving the set of equations for $\{\mathbf{z},\mathbf{R},\mathbf{P}\}$ as a function of the time t yields the evolving molecular state that describes the processes that take place during the collision. For the purpose of discussing charge exchange, we make use of the Mulliken population analysis [34]. From Eqs. (6) and (7), the number of electrons in the system is given by

$$N = \sum_{\nu,\mu} P_{\mu\nu}\Delta_{\nu\mu} = \sum_{\mu} (\mathbf{P}\Delta)_{\mu\mu} = \mathrm{Tr}(\mathbf{P}\Delta) \tag{14}$$

where $P_{\nu\mu}=\Sigma_i^N z_{i\nu}z_{i\mu}$, and $\Delta_{\mu\nu}$ is the atomic orbital overlap matrix. It is possible to interpret $(\mathbf{P}\Delta)_{\mu\mu}$ as the number of electrons to be associated with the basis function u_μ. From this, $n_A=\Sigma_{\nu\in A}(\mathbf{P}\Delta)_{\nu\nu}$ is the number of electrons associated with atom A. Thus, at any given time, we can calculate the electron population and probability of electron capture for the system or an atomic center.

Calculations are carried out using the ENDYNE program package [35].

IV. CALCULATIONS

For each projectile trajectory, the target was placed at the origin of a Cartesian laboratory coordinate system with the initial projectile velocity parallel to the z axis, and directed toward the target with an impact parameter b, measured along the x axis.

The atomic target is initially in its electronic ground state as computed in the given basis. The basis functions used for the atomic orbital expansion are derived from those optimized by Dunning [36]. For each of the nuclei, the electronic structure is described using a basis set consisting of $[5s5p2d/5s5p2d]$ Gaussian orbitals, supplemented with diffuse s and p orbitals for a better description of the longer range interaction. This produces a basis set with rank $K=36$ per atomic center, which, combined with the ETF and the supermolecular description of the electronic structure, makes a good description of the electronic excitation and low-ionization region of the interacting system. This basis set provides converged results for all the surveyed projectile energies. The impact parameters b range from 0.0 to 15.0 a.u., which we separate into three regions. For close collisions, from 0.0 to 6.0 a.u., we use steps of 0.1 a.u. For the intermediate region, from 6.0 to 10.0 a.u., we use steps of 0.5 a.u., and for $b>10.0$, we use steps of 1.0. This gives us 74 fully dynamical trajectories for each initial energy and molecular orientation. The projectile energies studied here range from 10 eV up to 300 keV.

The projectile is started 30 a.u. from the target, and the trajectory is evolved under the dynamical equations until the projectile is 30 a.u. past the target, or until there are no longer changes in the energy, velocity, or charge of the projectile. Thus, after the dynamics is finished for each trajectory, one obtains the total wave function, the nuclear positions, and momenta, and, therefore, one is able to calculate the deflection function Θ and the system's electronic properties, e.g., charge transfer and energy loss.

V. THE STOPPING CROSS SECTION

Our main goal in this work is to understand the process of energy loss suffered by protons and antiprotons when they collide with a hydrogen atom, and by which modes energy is transferred to the target. The stopping power, or energy loss per unit length for a projectile of energy E_p, can be written in terms of a differential scattering cross section $d\sigma/d\Omega$ as

$$S(E_p) = -\frac{1}{n}\frac{dE}{dx} = -\int \Delta E(E_p,\Omega)\frac{d\sigma}{d\Omega}d\Omega$$
$$= -\int b\Delta E(E_p,b)db\,d\varphi \tag{15}$$

where n is the density of target scattering centers, and ΔE is the kinetic energy loss of the projectile. Here, we have used the deflection function $\Theta(b)$ to transform the angular integral to the impact parameter representation.

Calculation of many trajectories at different impact parameters for each given incident energy yields the energy-dependent deflection function and energy loss, which can then, through Eq. (15), be used to calculate the stopping cross section and its electronic and nuclear contributions.

A. Deflection function

Figure 1 shows the deflection function $\Theta(b)$ as a function of impact parameter b for protons and antiprotons at two typical projectile energies 0.5 and 5.0 keV/amu. There is a well behaved deflection function for proton scattering, which exhibits a glory angle near 4 a.u. and a shallow rainbow near $b=6.0$ a.u. for $E_p=5.0$ keV. For $E_p=0.5$ keV, the glory angle occurs at $b\sim5$ a.u. and the rainbow angle at $b\sim6.2$. In the case of the antiproton, there is always an attraction with a maximum which could be considered a rainbow. At large b, the attraction is small, but at intermediate b, the screening of the electron is reduced when the antiproton penetrates the H electron cloud and thus the attraction strengthens. This is a result of the nonclassical trajectories resulting from the electron-nuclear coupling during the dynamics, particularly at close distances.

B. Electron transfer cross section

Much of the analysis of stopping power, and especially of Eqs. (1) and (2), assumes a fully stripped, or at least constant

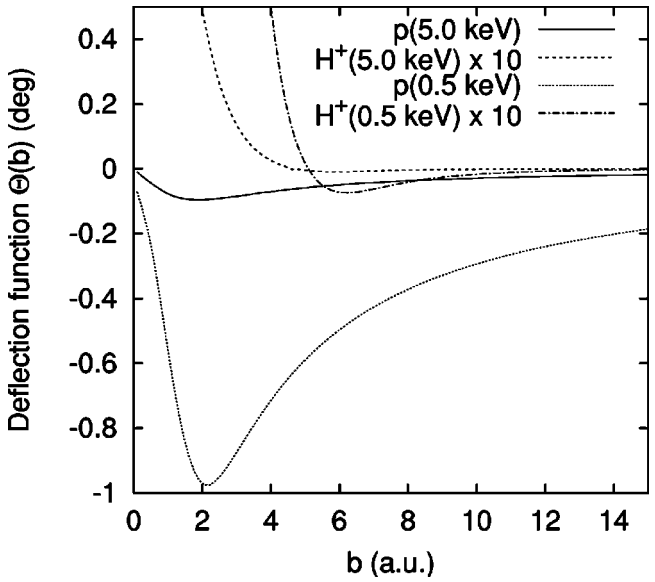

FIG. 1. Calculated deflection functions for protons and antiprotons on hydrogen at 5.0 and 0.5 keV/amu. Note that the proton deflection functions have been scaled by a factor of 10 to emphasize the rainbow and glory angle (attractive and repulsive regions of the interaction).

charge, projectile. However, due to quantum mechanical interaction between the projectile and the target, one expects electron exchange among the collision partners. From the evolving molecular-state wave function, one can calculate the probability for electron capture or loss. From the probability for charge exchange, the charge exchange cross section can be obtained from

$$\sigma_{exch}(E_p) = 2\pi \int_0^\infty P_{exch}(b,E_p) b\, db. \tag{16}$$

The charge exchange cross section for $H^+ \rightarrow H$ has been reported in Ref. [37], and it is clear that an antiproton will not pick up an electron during the collision [38], which is verified by our calculations. The resonant charge transfer between a H^+ and a hydrogen atom ensures a large charge transfer cross section as the velocity of the projectile slows down. A good description of the electron transfer and the dynamics of the collision is thus required for a proper account of the projectile energy loss at low projectile energies. As reported in Ref. [37], END provides an excellent description of the dynamics of resonant charge exchange for protons colliding on hydrogen in a consistent manner through all the projectile energies under consideration, contrary to other studies where several velocity-dependent methods have been used [19]. Animations of $H^+ \rightarrow H$ and $\overline{p} \rightarrow H$ for collisions at $E_p = 10$ keV and at $b = 1$ a.u. can be seen in [39] where both a contour map and its two-dimensional projection are shown. The polarization of the charge cloud as the projectile approaches is evident, and there is some charge loss to the proton, as expected.

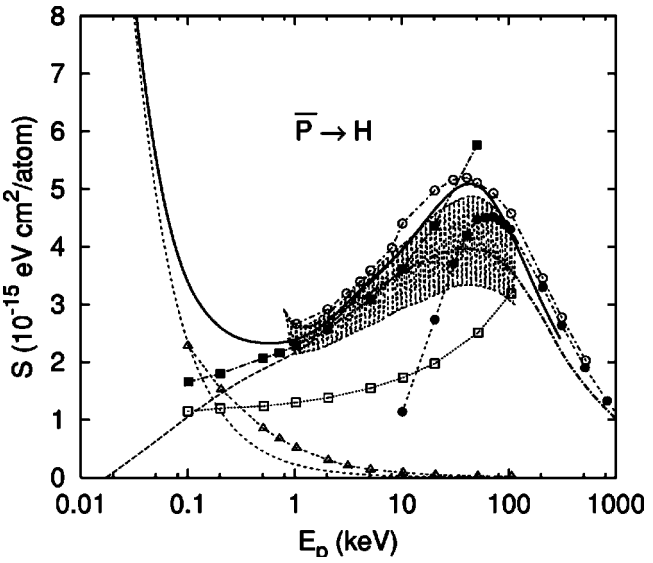

FIG. 2. Calculated total stopping cross sections for antiprotons on atomic hydrogen targets. The solid line is the total stopping cross section according to END. The long dashed line is the electronic contribution and the short dashed line is the nuclear contribution. The dashed area with the best fit represented by the dot-dashed line shows the experimental data from Adamo *et al.* [24]. The symbols are the different models employed by Schiwietz *et al.* [18]. The solid boxes are the AI results; the open circles are the AO results; the full circles are the DW model; the open squares are the AI for molecular hydrogen; and the open triangles are the nuclear stopping cross section.

VI. THE BARKAS (Z_1^3) CORRECTION

In Fig. 2, we present the stopping cross sections calculated for antiprotons colliding with hydrogen atoms. The solid thick line is our total antiproton stopping, the long dashed line is its electronic component, and the short dashed line is its nuclear component. As the calculations we present do not contain relativistic effects, the annihilation expected to occur at lower energies is not seen. The results are compared to the H_2 molecular experiments of Adamo *et al.* [24] which are represented by the dot-dashed line. The error bars are represented by the shaded area. We note an overestimation when comparing our data to the experimental results, but within the experimental error bars. An explanation might be that the experimental data are for a molecular target, when our results are for atomic hydrogen, thus neglecting the effect of the molecular bonding, particularly at low projectile energies. This is also concluded in Ref. [19]. At higher projectile energies our agreement is better, as expected. In the same figure, we compare our results with those of Schiwietz *et al.* [19]. We note that at high energies, the AO and END methods compare relatively well, with the END results closer to the experimental data. The DW method agrees well at high energies, but fall short in the intermediate region. At low projectile energies, the AI method has a trend similar to END; however, it breaks at higher energies. Finally, the nuclear stopping cross sections follow the same trend in all methods although quantitatively they are different. The reason seems to be the approach used for accounting for the

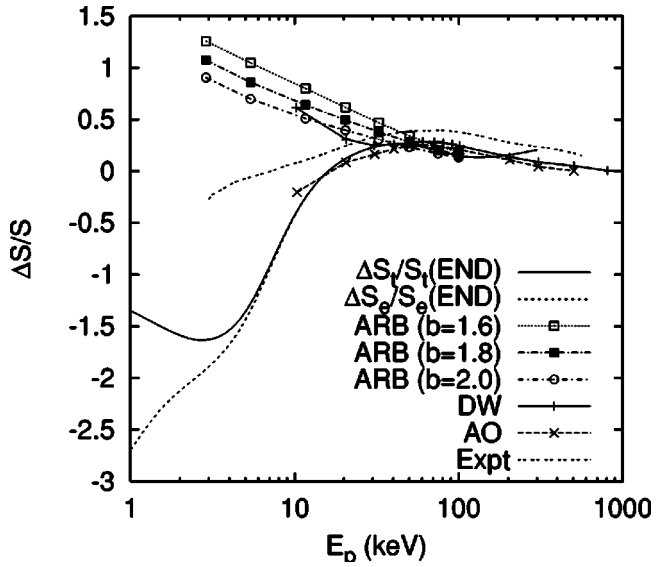

FIG. 3. Relative stopping cross section for antiprotons and protons colliding with hydrogen atoms as obtained by END. Also, we show the results from the ARB theory (Barkas correction) [Eq. (3)], and those reported in Ref. [19] for the AO and DW models.

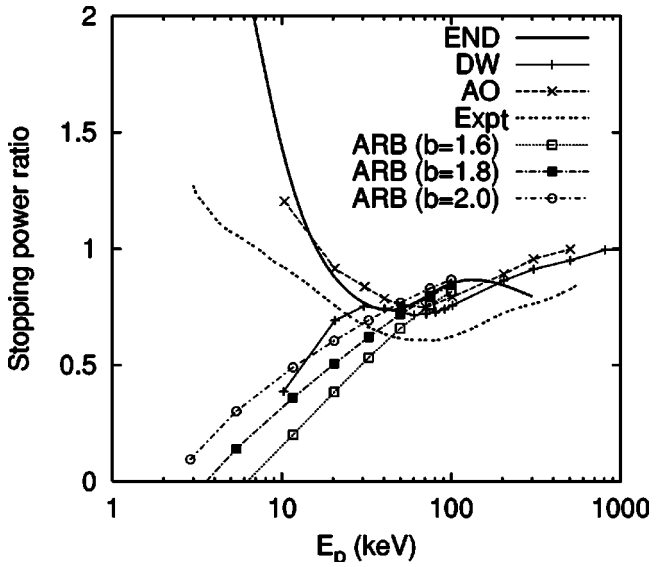

FIG. 4. The same as Fig. 3, but for the stopping cross section ratio of antiprotons and protons colliding with hydrogen atoms.

coupling of the electronic and nuclear degrees of freedom. In particular, we note that at low projectile energies, impact parameters lower than the Fermi-Teller radius [40] $R_{FT}=0.639$ a.u. produce ionization, as expected [19,38]. However, for larger impact parameters ($b>R_{FT}$) the electron remains bound and repels the incoming projectile in a billiard-ball-like collision when coupled to the hydrogen nuclei. These impact parameters are largely responsible for the large nuclear stopping cross section.

As mentioned previously, the relative difference of the stopping cross sections between the proton and antiproton projectiles shows the leading contribution to be the Barkas term at high energies if the higher contributions are assumed small. In Fig. 3, we present the relative difference between the proton and antiproton stopping cross section for collisions with atomic hydrogen, as obtained from our data from Fig. 2, and those reported in Ref. [37] for H^+ colliding on atomic hydrogen. Here the solid line is the total Barkas correction and the dashed line is its electronic component from our calculations. In addition, we have included the Barkas results calculated by Ashley, Ritchie, and Brandt [14–17] for atomic hydrogen targets for the three different values of the empirical parameter b of their theory ($b=1.6$, 1.8, and 2.0). In the ARB approach, the stopping cross section is given by

$$S(x) = S_0(x)[1 + Z_1 B(x)], \tag{17}$$

where $x=v^2/v_0^2 Z_2$, v being the projectile velocity and v_0 the Bohr velocity. Here S_0 is the first Born term, and $B(x)=\kappa(b,x)/Z_2^{1/2}x$ is the Barkas term. The function $\kappa(b,x)$ is tabulated in Ref. [15]. This approach assumes that higher orders in Z_1 are insignificant. Thus, the relative value of the stopping cross section is given by

$$\frac{\Delta S}{S} = \frac{2Z_1 B(x)}{1 + Z_1 B(x)}, \tag{18}$$

which depends only on the Barkas term $B(x)$. Figure 3 shows that the END and the ARB results agree with the expected high-velocity behavior of the Barkas correction. However, for low projectile energies, other effects start to overwhelm the pure Barkas term. Of these, charge exchange (electron capture) is the most predominant for the case of protons. This is reported in Ref. [37] at low projectile energies, where the charge exchange cross section is largest for protons but is absent in the antiproton case. We also note that there may be effects due to L_{2i+1}, $i>1$, terms contributing at low energies which are taken into account in the END approach. This is observed in Fig. 3 for projectile energies below 10 keV where there is a change in sign of $\Delta S/S$ contrary to the predictions of the ARB model. To the best of our knowledge, there have been no systematic studies of terms of order higher than L_2 in the Born series. We hope our results foster more work in that direction. Also, in the same figure, we show the results of the DW and AO models, as reported by Schiwietz *et al.* [19]. We note that the AO and END results agree relatively well for all the reported projectile energies. Also, we note that the AO model shows the same change in sign of $\Delta S/S$, thus incorporating higher orders in the stopping cross section.

In Fig. 4, we show the stopping power ratio, where we note a good agreement between END and AO results. However, from these results is hard to observe a change of sign of the Barkas term.

VII. SUMMARY

We have calculated the stopping cross sections of atomic hydrogen for antiprotons at low to intermediate projectile energies by means of a nonperturbative, nonadiabatic approach. The explicit difference between the proton and anti-

proton stopping cross sections gives the Barkas effect at high energies and higher contributions at lower projectile energies, which we report and compare to direct calculations of the effect by Ashley, Ritchie, and Brandt, as well as those reported by Schiwietz *et al.* through the AI, DW, and AO models. The agreement between the AO, ARB, and our results is fairly good for energies $E_p > 30$ keV. For the lower-energy region, electron capture effects start to become important. We find that at low projectile energies, ionization, combined with a repulsive billiard-ball-like collision, is responsible for most of the stopping cross section.

ACKNOWLEDGMENTS

This work was supported in part by NSF (Grant No. CHE-9732902 to N.Y.O.), by ONR (Grants No. N0014-00-1-0197 to N.Y.O. and No. N00014-96-1-0707 to J.R.S.), and by the IBM SUR program.

[1] Mme. Pierre Curie, C. R. Hebd. Seances Acad. Sci. **130**, 76 (1900).
[2] J. J. Thomson, Philos. Mag. **6–23**, 449 (1912).
[3] N. Bohr, Philos. Mag. **25**, 10 (1913).
[4] N. Bohr, Philos. Mag. **30**, 581 (1915).
[5] H. Bethe, Ann. Phys. (Leipzig) **5**, 325 (1930).
[6] H. Bethe, Z. Phys. **76**, 293 (1932).
[7] H. Bethe, Phys. Rev. **89**, 1256 (1953).
[8] R. Cabrera-Trujillo, S. Cruz, J. Oddershede, and J. Sabin, Phys. Rev. A **55**, 2864 (1997).
[9] J. Lindhard, Nucl. Instrum. Methods **132**, 1 (1976).
[10] W. H. Barkas, J. N. Dyer, and H. H. Heckman, Phys. Rev. Lett. **11**, 26 (1963).
[11] G. Basbas, Nucl. Instrum. Methods Phys. Res. B **4**, 227 (1984).
[12] M. Inokuti, Nucl. Tracks Radiat. Meas. **16**, 115 (1989).
[13] J. D. Jackson and R. L. McCarthy, Phys. Rev. B **6**, 4131 (1972).
[14] J. C. Ashley, R. H. Ritchie, and W. Brandt, Phys. Rev. B **5**, 2393 (1972).
[15] J. C. Ashley, R. H. Ritchie, and W. Brandt, Phys. Rev. A **8**, 2402 (1973).
[16] J. C. Ashley, R. H. Ritchie, and W. Brandt, Phys. Rev. A **10**, 737 (1974).
[17] R. H. Ritchie and W. Brandt, Phys. Rev. A **17**, 2102 (1978).
[18] G. Schiwietz, U. Wille, R. Diez-Muiño, P. D. Fainstein, and P. L. Grande, Nucl. Instrum. Methods Phys. Res. B **115**, 106 (1996).
[19] G. Schiwietz, U. Wille, R. Díez-Muiño, P. D. Fainstein, and P. L. Grande, J. Phys. B **29**, 307 (1996).
[20] N. R. Arista and A. F. Lifschitz, Phys. Rev. A **59**, 2719 (1999).
[21] H. Bichsel, Phys. Rev. A **65**, 052709 (2002).
[22] P. Sigmund and A. Schinner, Nucl. Instrum. Methods Phys. Res. B **212**, 110 (2003).
[23] R. Schmidt, H. Daniel, F. J. Hartmann, P. Hauser, F. Kottmann, M. Muhlbauer, C. Petitjean, W. Schott, D. Taqqu, and P. Wojciechowski, Eur. Phys. J. D **3**, 119 (1998).
[24] A. Adamo *et al.*, Phys. Rev. A **47**, 4517 (1993).
[25] S. P. Møller, E. Uggerøj, H. Bluhme, H. Knudsen, U. Mikkelsen, K. Paludan, and E. Morenzoni, Phys. Rev. A **56**, 2930 (1997).
[26] E. L. Rizzini *et al.*, Phys. Rev. Lett. **89**, 183201 (2002).
[27] Y. Öhrn, E. Deumens, A. Diz, R. Longo, J. Oreiro, and H. Taylor, *Time-Dependent Quantum Molecular Dynamics* (Plenum, New York, 1992).
[28] E. Deumens, A. Diz, R. Longo, and Y. Öhrn, Rev. Mod. Phys. **66**, 917 (1994).
[29] E. Deumens and Y. Öhrn, J. Phys. Chem. **92**, 3181 (1988).
[30] E. Deumens, A. Diz, H. Taylor, and Y. Öhrn, J. Chem. Phys. **96**, 6820 (1992).
[31] J. B. Delos, Rev. Mod. Phys. **53**, 287 (1981).
[32] D. J. Thouless, Nucl. Phys. **21**, 225 (1960).
[33] J. R. Klauder and B. S. Skagerstman, *Coherent States, Applications in Physics and Mathematical Physics* (World Scientific, Singapore, 1985).
[34] R. S. Mulliken, J. Chem. Phys. **36**, 3428 (1962).
[35] E. Deumens, T. Helgaker, A. Diz, H. Taylor, J. Oreiro, B. Mogensen, J. A. Morales, M. C. Neto, R. Cabrera-Trujillo, and D. Jacquemin, computer code ENDYNE, Quantum Theory Project, University of Florida, Gainesville FL 32611-8435, 2000.
[36] T. H. Dunning, J. Chem. Phys. **90**, 1007 (1989).
[37] R. Cabrera-Trujillo, Y. Öhrn, E. Deumens, and J. R. Sabin, J. Chem. Phys. **116**, 2783 (2002).
[38] P. S. Krstić, D. R. Schultz, and R. K. Janev, J. Phys. B **29**, 1941 (1996).
[39] http.//www.qtp.ufl.edu/flib.html
[40] E. Fermi and E. Teller, Phys. Rev. **72**, 399 (1947).